Acta Crystallographica Section B
Structural Science
ISSN 0108-7681

Synchrotron powder diffraction in a systematic study of 4′-[2-(tosylamino)benzylideneamino]-2,3-benzo-15-crown-5 complexes

Andrey V. Dorokhov,[a] Dmitrii Yu. Chernyshov,[b] Anatolii S. Burlov,[c] Alexandr D. Garnovskii,[c] Irina S. Ivanova,[d] Elena N. Pyatova,[d] Aslan Yu. Tsivadze,[a] Leonid A. Aslanov[e] and Vladimir V. Chernyshev[a,e]*

[a]A. N. Frumkin Institute of Physical Chemistry and Electrochemistry, Leninsky prospect 31, 119991 Moscow GSP-1, Russia, [b]ESRF, BP 220, F-38043, Grenoble CEDEX, France, [c]Research Institute of Physical and Organic Chemistry, Rostov State University, ul. Stachki, 194/2, 344090 Rostov-on-Don, Russia, [d]N. S. Kurnakov Institute of General and Inorganic Chemistry, Leninsky prospect 31, 119991 Moscow GSP-1, Russia, and [e]Department of Chemistry, Moscow State University, 119992 Moscow, Russia

Correspondence e-mail: vladimir@struct.chem.msu.ru

Received 12 July 2006
Accepted 24 January 2007

The crystal structures of two compounds, CuL_2 and LiNCS·HL [HL = 4′-[2-(tosylamino)benzylideneamino]-2,3-benzo-15-crown-5], have been determined from synchrotron powder diffraction data. Both compounds crystallize in the monoclinic space group $P2_1/c$ and with one molecule in the asymmetric unit. In CuL_2 the four N atoms of two bidentate L ligands coordinate the Cu^{II} ion in a distorted tetrahedral geometry with Cu—N distances of 1.98 (5)–2.05 (5) Å, while two O atoms from two sulfoxide groups complete the distorted octahedral Cu coordination [Cu—O 2.64 (4), 2.74 (4) Å]. In LiNCS·HL, lithium is coordinated by all five ether O atoms with Li—O distances of 2.03 (3)–2.50 (3) Å and an N atom from the thiocyanate moiety [Li—N 1.98 (3) Å] in a distorted pentagonal pyramidal geometry. Preliminary potentiometric selectivity measurements for ion-selective electrodes (ISEs) based on CuL_2 and ZnL_2 demonstrated significant differences in their selectivity. In order to find a possible reason for this, theoretical calculations at the DFT (B3LYP) level were performed. These calculations used the crystal structures of CuL_2, LiNCS·HL, ZnL_2 and HL as input geometries for the minimum energy optimization *in vacuo*. The results indicate that in ML_2 complexes (M = Cu, Zn) the electronic structure of the metal ion determines the spatial orientation of benzo-15-crown-5 macrocycles, and their different orientation in CuL_2 and ZnL_2 results in different potentiometric selectivities of ISEs based on these compounds.

1. Introduction

In recent years macrocyclic polyethers have attracted much attention in many areas of science and technology (Izatt & Christensen, 1978; Inoue & Gokel, 1990; Fedorova *et al.*, 2001; Bren, 2001; Tsivadze, 2004). Very recent investigations have shown that crown ethers can effectively be used in pharmaceutical applications of chiral capillary electrophoresis as chiral selectors (Amini, 2001; Ha *et al.*, 2006), for the transportation of a protein from an aqueous phase to ionic liquids (Shimojo *et al.*, 2006), as supramolecular optical chemosensors (Bell & Hext, 2004) and in many other areas (Gokel *et al.*, 2004; Cook *et al.*, 2005; Mazik *et al.*, 2006). One of the successful and well known applications of crown ethers in analytical chemistry is ion transfer and ion recognition, particularly as neutral carriers in ion-selective electrodes (ISE; Bakker *et al.*, 1997; Bühlmann *et al.*, 1998). To improve or enhance the ion selectivity of crown ethers, a number of novel macrocycles have been designed and synthesized in recent years (Liu *et al.*, 2000, and references therein; Gokel *et al.*, 2004, and references therein). The synthesis of new ligands

having two or more donor centers has attracted special attention (Van Veggel *et al.*, 1994; Gonzalez-Lorenzo *et al.*, 2003; Sousa *et al.*, 2004), which will allow the creation of new polyfunctional materials.

Of specific interest to our group is the design and synthesis of azomethine derivatives of benzo-15-crown-5 ether and their complexes along with the structural characterization of the compounds obtained (Minacheva, Ivanova, Dorokhov *et al.*, 2004; Minacheva, Ivanova, Pyatova *et al.*, 2004; Ivanova *et al.*, 2005; Minacheva *et al.*, 2006). Recently, we reported the synthesis and solid-state structures of the 4′-[2-(tosylamino)-benzylideneamino]-2,3-benzo-15-crown-5 (H*L*) ligand (Minacheva, Ivanova, Dorokhov *et al.*, 2004) and its ZnL_2 complex (Minacheva *et al.*, 2006). We have also synthesized the CuL_2 and LiNCS·H*L* complexes, which did not yield single crystals suitable for X-ray crystal structure determination but were obtained only as crystalline powders. Preliminary potentiometric selectivity measurements for the ion-selective electrodes (ISEs) based on H*L*, ZnL_2 (Ivanova *et al.*, 2007*a*) and CuL_2 (Ivanova *et al.*, 2007*b*) demonstrated significant differences in their selectivity

$$\begin{aligned}
\mathrm{H}L &: \mathrm{Pb^{2+}} > \mathrm{Ag^{+}} > \mathrm{K^{+}} > \mathrm{Rb^{+}} > \mathrm{Cu^{2+}} > \mathrm{Na^{+}} \simeq \mathrm{Cs^{+}} \\
&\simeq \mathrm{Sr^{2+}} > \mathrm{NH_4^{+}} \\
\mathrm{Zn}L_2 &: \mathrm{Ag^{+}} > \mathrm{Pb^{2+}} > \mathrm{K^{+}} > \mathrm{Cu^{2+}} > \mathrm{Rb^{+}} > \mathrm{Cs^{+}} \simeq \mathrm{Ba^{2+}} \\
&\simeq \mathrm{Na^{+}} \simeq \mathrm{NH_4^{+}} \\
\mathrm{Cu}L_2 &: \mathrm{Cu^{2+}} > \mathrm{K^{+}} > \mathrm{NH_4^{+}} > \mathrm{Na^{+}} > \mathrm{Rb^{+}} \simeq \mathrm{Cs^{+}} > \mathrm{Pb^{2+}} \\
&> \mathrm{Ba^{2+}} > \mathrm{Ag^{+}}.
\end{aligned}$$

A possible reason for the different selectivity of these three compounds may be the different geometry of the molecules and the conformation of the macrocycles. This encouraged us to solve the crystal structures of the complexes in the hope of finding a correlation between their structure and potentiometric selectivity. Here we present the crystal structure of the CuL_2 complex determined by powder diffraction methods (David *et al.*, 2002; Baerlocher & McCusker, 2004). The crystal structure of the LiNCS·H*L* complex was also determined to estimate the conformational flexibility of the H*L* ligand in the case of the cation binding to the macrocycle.

2. Experimental

2.1. Synthesis

N-(4′-Benzo-15-crown-5)-2-(amino-*N*-tosyl)-phenylaldimine (H*L*) and its complexes were prepared as depicted below according to the published procedures for H*L* (Minacheva, Ivanova, Dorokhov *et al.*, 2004), CuL_2 and ZnL_2 (Minacheva *et al.*, 2006), and LiNCS·H*L* (Ivanova *et al.*, 2005; also see the supplementary materials[1] for details of the synthesis).

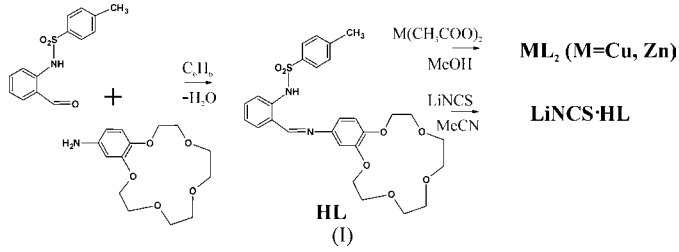

2.2. Potentiometric measurements

2.2.1. Membranes and ISEs preparation. The neutral carrier (H*L*, ZnL_2 or CuL_2), plasticizer (*o*-nitrophenyloctyl ether, Fluka) and high molecular-weight polyvinylchloride (PVC; Aldrich) were dissolved in the appropriate volume of cyclohexanone and mechanically stirred. All membrane cocktails were cast in glass rings placed on glass plates. Solvent from PVC membrane was allowed to evaporate for a week at room temperature. The thickness of the resulting membranes was about 0.2–0.3 mm. Small disks were punched from the cast membranes and mounted in electrode bodies.

2.2.2. Measurements. The electrochemical properties of the membranes were investigated in the conventional configuration. The external reference electrode was a double-junction Ag/AgCl OP-8020 P (Radelkis). The electrochemical potential was measured using a pH/ion analyzer OP-300 (Radelkis, Hungary). The selectivity coefficients were determined by the separate solution method (IUPAC, 1976) using 0.01 mol l^{-1} solutions of metal chlorides or nitrates.

2.3. DFT calculations

Density functional theory (DFT) calculations for the free H*L* ligand and the three complexes ZnL_2, CuL_2 and LiNCS·H*L* *in vacuo* were performed using the *PRIRODA* program (Laikov, 1997) employing the B3LYP exchange-correlation function (Becke, 1988; Lee *et al.*, 1988). For representation of the Kohn–Sham one-electron wavefunctions, sets of contracted Gaussian-type functions were used; the contracted patterns were (311/1) for H, (51111/31) for Li, (611111/411/11) for C, N and O, (6111111111/5111111/11) for S, (711111111111/511111111/5111) for Cu, and (7111111111111/5111111111/5111) for Zn. For the CuL_2 system, only the configuration S = 1/2 has been taken into account. The geometry optimization was performed using the quasi-Newton method to the final gradient of 3×10^{-5} Hartree Å^{-1}. The *in vacuo* optimized Cartesian coordinates obtained for the systems described in this paper are given in the supplementary materials.

2.4. Crystal structure determination

2.4.1. Data collection and indexing. Preliminary powder diffraction measurements were carried out on a laboratory Guinier–Huber camera. The laboratory patterns revealed a good degree of crystallinity for both compounds, but did not

[1] Supplementary data for this paper are available from the IUCr electronic archives (Reference: KD5008). Services for accessing these data are described at the back of the journal.

Table 1
Experimental details.

	Cu*L*$_2$	LiNCS·H*L*	H*L*†	Zn*L*$_2$‡
Crystal data				
Chemical formula	$C_{56}H_{62}CuN_4O_{14}S_2$	$C_{29}H_{32}LiN_3O_7S_2$	$C_{28}H_{32}N_2O_7S$	$C_{56}H_{62}N_4O_{14}S_2Zn$
M_r	1142.79	605.66	540.63	1144.62
Cell setting, space group	Monoclinic, $P2_1/c$	Monoclinic, $P2_1/c$	Monoclinic, $P2_1/c$	Monoclinic, $C2/c$
Temperature (K)	295 (2)	295 (2)	295 (2)	295 (2)
a, b, c (Å)	19.0356 (6), 17.4332 (6), 17.4180 (6)	9.2918 (3), 23.0117 (7), 15.2798 (5)	12.781 (1), 25.017 (9), 8.859 (1)	23.139 (2), 19.931 (2), 14.604 (2)
β (°)	113.824 (3)	108.063 (2)	108.20 (2)	121.20 (1)
M_{20}	53	65	–	–
V (Å^3)	5287.7 (3)	3106.11 (17)	2691 (1)	5760.9 (5)
Z	4	4	4	4
D_x (Mg m^{-3})	1.436	1.295	1.334	1.320
Radiation type	Synchrotron	Synchrotron	Mo $K\alpha$	Mo $K\alpha$
μ (mm^{-1})	0.30	0.12	–	–
Specimen form, colour	Cylinder (particle morphology: no specific habit), black	Cylinder (particle morphology: no specific habit), yellow	–	–
Specimen size (mm)	15 × 0.3 × 0.3	15 × 0.3 × 0.3	–	–
Specimen preparation pressure (kPa)	101.3 (2)	101.3 (2)	–	–
Specimen preparation temperature (K)	295 (2)	295 (2)	–	–
Data collection				
Diffractometer	ESRF powder diffractometer	ESRF powder diffractometer	–	–
Data collection method	Specimen mounting: specimen was sealed in a 0.3 mm diameter borosilicate glass capillary; mode: transmission; scan method: continuous	Specimen mounting: specimen was sealed in a 0.3 mm diameter borosilicate glass capillary; mode: transmission; scan method: continuous	–	–
Absorption correction	None	None	–	–
2θ (°)	$2\theta_{min}$ = 1.017, $2\theta_{max}$ = 22.014, increment = 0.003	$2\theta_{min}$ = 3.024, $2\theta_{max}$ = 23.024, increment = 0.004	$2\theta_{min}$ = 0, $2\theta_{max}$ = 46	$2\theta_{min}$ = 0, $2\theta_{max}$ = 50
Refinement				
Refinement on	I_{net}	I_{net}	–	–
R_p§	0.0462	0.0435	–	–
	0.0447	0.0368	–	–
R_{wp}	0.0627	0.0545	–	–
	0.0593	0.0461	–	–
R_{exp}	0.0481	0.0274	–	–
Goodness-of-fit	1.30	1.98	–	–
Wavelength of incident radiation (Å)	0.51966 (1)	0.52000 (1)	–	–
Excluded region(s)	None	None	–	–
Profile function	Split-type pseudo-Voigt (Toraya, 1986)	Split-type pseudo-Voigt (Toraya, 1986)	–	–
No. of parameters	277	213	–	–
H-atom treatment	Not refined	Not refined	–	–
Weighting scheme	Based on measured s.u.'s	Based on measured s.u.'s	–	–
$(\Delta/\sigma)_{max}$	0.027	0.035	–	–
Preferred orientation correction	March–Dollase texture correction (Dollase, 1986). Direction of preferred orientation: 100, texture parameter r = 0.94 (2)	March–Dollase texture correction (Dollase, 1986). Direction of preferred orientation: 001, texture parameter r = 0.910 (9)	–	–

Computer programs used: *MRIA* (Zlokazov & Chernyshev, 1992), *PLATON* (Spek, 2003). † Minacheva, Ivanova, Dorokhov *et al.* (2004). ‡ Minacheva *et al.* (2006). § R_p, R_{wp} and R_{exp} are defined according to Young & Wiles (1982). The results of the final bond-restrained Rietveld refinement are given in the first row of each pair of rows and the results of the Pawley fit are given in the second row of each pair.

allow indexing. High-resolution synchrotron powder diffraction data were collected at the powder diffraction station BM01B (Swiss–Norwegian beamlines at the European Synchrotron Radiation Facility). The powder was placed in a 0.3 mm glass capillary and diffraction patterns were measured in Debye–Scherrer geometry at room temperature. Owing to the choice of wavelength, the low-angle region $2\theta < 3°$ for LiNCS·H*L* was not accessible, so the *d* spacings of the two first peaks (12.270 and 11.501 Å) were taken from a laboratory pattern for indexing purposes. The monoclinic unit-cell dimensions of LiNCS·H*L* and CuL_2 were determined using three indexing programs: *TREOR*90 (Werner *et al.*, 1985), *ITO*

(Visser, 1969) and *AUTOX* (Zlokazov, 1992, 1995). Based on systematic extinctions the space group for both compounds was determined to be $P2_1/c$. The unit-cell parameters and space groups were further tested using Pawley's fit (Pawley, 1981) and confirmed by crystal structure solution. The crystallographic data for LiNCS·H*L* and CuL_2 are given in Table 1.

2.4.2. Structure solution.. The crystal structures have been solved by a combination of simulated annealing (Zhukov *et al.*, 2001) and grid-search (Chernyshev & Schenk, 1998) techniques; detailed methodology is described elsewhere (International Union of Crystallography Newsletter, 2004).

LiNCS·H*L*: The initial molecular model for *L* without H atoms was taken from the single-crystal structure of H*L* (Minacheva, Ivanova, Dorokhov *et al.*, 2004; CSD refcode DANREQ). However, the conformation of the macrocycle was changed to a more 'planar' configuration to be in accordance with that observed in the related structure found in the Cambridge Structural Database (CSD, Version 5.27; Allen, 2002), where the 15-crown-5 macrocycle binds the Li^+ cation (Nurtaeva & Holt, 1999; CSD refcode BEQREU). The only torsional degree of freedom allowed for *L* at the beginning of the structure solution process was the rotation of the tosyl group around the N9—S8 bond (Fig. 1). The geometrical parameters of the LiNCS moiety were taken from the literature (Dale *et al.*, 1987; *CSD* refcode *FOBHEJ*) and fixed. The simulated annealing was used in a preliminary search for possible solutions; 12 degrees of freedom – three translational, three rotational and one torsional parameters for *L*, three translational and two rotational parameters for the LiNCS were varied and 300 X_{obs} (Chernyshev & Schenk, 1998) low-angle values were used. After each simulated annealing run, the obtained orientations of *L* and LiNCS were fixed and used in a translational grid search with 0.4 Å grids. This combination of simulated annealing and grid-search techniques was applied several times and allowed the finding of the preferred position and orientation for the LiNCS moiety, which were further fixed. Two more internal degrees of freedom for *L* were added – the limited rotations around the C16—N17 and C2—S8 bonds (Fig. 1). The simulated annealing and grid-search techniques were independently used in a search for the position and orientation of *L* by varying nine degrees of freedom, and both gave only one solution. The correctness of the solution was later checked by the restraint-free Rietveld refinement without H atoms; in spite of some distortions of the bond lengths and angles the results were the same.

Cu L_2: The initial molecular model without H atoms was taken from the single-crystal structure of ZnL_2 (Minacheva *et al.*, 2006). Three internal degrees of freedom were allowed for CuL_2; rotation of the tosyl group around the N9*A*—S8*A* and N9*B*—S8*B* bonds, respectively, and limited variation of the dihedral angle between the N9*A*/Cu1/N17*A* and N9*B*/Cu1/N17*B* planes (Fig. 2). Following the aforementioned case of LiNCS·H*L*, the simulated annealing and grid-search procedures were tested by varying nine degrees of freedom and using 300 X_{obs} low-angle values. However, no acceptable solutions were obtained. Therefore, the strategy of structure solution was changed and concentrated first on the location of the Cu atom, using the grid-search technique applied to the whole powder pattern and further tested by the Rietveld refinement. The unique position of Cu was found and fixed, then the orientations of the ligands with four additional internal degrees of freedom; namely, limited rotations around the C16*A*—N17*A*, C2*A*—S8*A*, C16*B*—N17*B* and C2*B*—S8*B* bonds (Fig. 2) were determined by simulated annealing using 300 X_{obs} values. The conformations of two 15-crown-5 macrocycles were established at the stage of structural refinement. Attempts to reveal the correctness of the solution by the restraint-free Rietveld refinement were useless, because of a large number of independent non-H atoms and weak counting statistics for CuL_2, compared with the case of LiNCS·H*L*. In addition, a specific relationship between the unit-cell dimensions ($a\sin\beta \simeq b \simeq c$) leads to severe overlapping of the peaks. As a result, many of the bond lengths and angles appeared to be chemically unreasonable in the restraint-free Rietveld refinement, although the positions of Cu and two S atoms were the same.

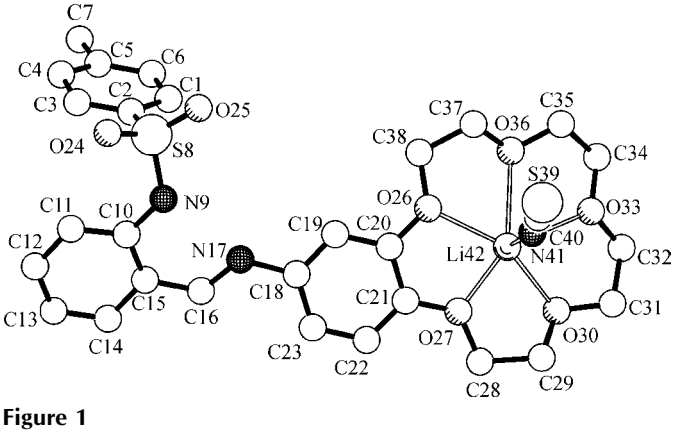

Figure 1
View of LiNCS·H*L* with the atom-numbering scheme. H atoms have been omitted for clarity.

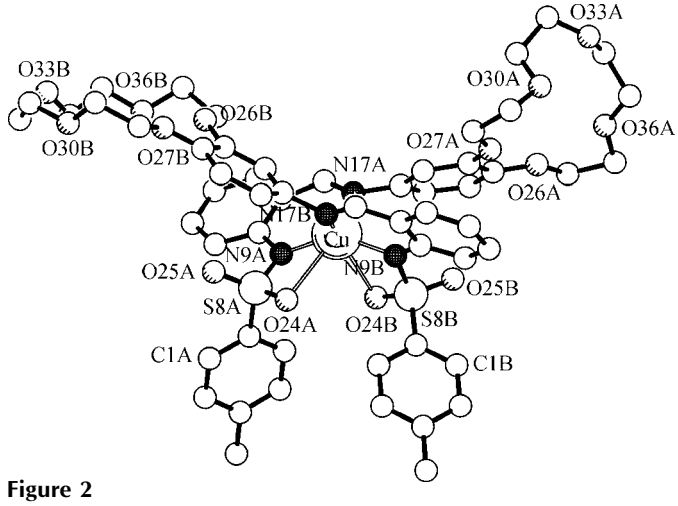

Figure 2
View of CuL_2 with the atom-numbering scheme. The numbering of C atoms in the ligands *A* and *B* corresponds to that in LiNCS·H*L*. H atoms have been omitted for clarity.

Table 2
Selected bond distances (Å) and angles (°) for CuL_2.

Cu—N9*A*	1.98 (5)	Cu—N9*B*	1.98 (5)
Cu—N17*A*	2.05 (5)	Cu—N17*B*	2.03 (5)
Cu—O24*A*	2.74 (4)	Cu—O24*B*	2.64 (4)
N17*A*—C18*A*	1.46 (9)	N17*B*—C18*B*	1.49 (8)
N17*A*—C16*A*	1.29 (8)	N17*B*—C16*B*	1.36 (8)
N9*A*—Cu—N17*A*	94 (2)	N9*B*—Cu—N17*B*	87 (2)
N9*A*—Cu—N17*B*	111 (2)	N9*B*—Cu—N17*A*	103 (2)
N9*A*—Cu—N9*B*	143 (2)	N17*A*—Cu—N17*B*	124 (2)
O24*A*—Cu—N9*A*	59.2 (15)	O24*B*—Cu—N9*B*	61.5 (17)
O24*A*—Cu—N17*A*	152.3 (18)	O24*B*—Cu—N17*B*	141.0 (16)
O24*A*—Cu—N9*B*	97.8 (19)	O24*B*—Cu—N9*A*	87.0 (18)
O24*A*—Cu—N17*B*	75.0 (18)	O24*B*—Cu—N17*A*	87.0 (17)
O24*A*—Cu—O24*B*	86.7 (11)		

2.4.3. Rietveld refinement. In the final bond-restrained Rietveld refinements the patterns were fitted with the program *MRIA* (Zlokazov & Chernyshev, 1992) using a split-type pseudo-Voigt peak-profile function (Toraya, 1986) and taking into account anisotropic line-broadening (Popa, 1998) and the March–Dollase texture formalism (Dollase, 1986). The refined values of the texture parameter *r* and the directions of the preferred orientations were 0.910 (9) and [001] for LiNCS·H*L*, and 0.94 (2) and [100] for CuL_2, respectively.

LiNCS·H*L*: Four isotropic displacement parameters were refined: two for the S8 and S39 atoms, respectively, one common parameter for the C40, N41 and Li42 atoms, and one common parameter for the remaining non-H atoms. Restraints were applied to the intramolecular bond lengths and contacts (< 2.6 Å) in the H*L* and LiNCS moieties. The strength of the restraints was a function of interatomic separation and, for intramolecular bond lengths, corresponded to an r.m.s. deviation of 0.03 Å. Additional restraints were applied to the planarity of the following fragments (Fig. 1):

(i) C1–C7, S8 (eight atoms),

(ii) N9, C10–C16 (eight atoms) and

(iii) N17, C18–C23, O26, O27 (nine atoms), with the maximal allowed deviation from the mean plane 0.1 Å.

CuL_2: Five isotropic displacement parameters were refined – three for Cu1, S8*A* and S8*B* atoms, respectively, and two common parameters for the remaining non-H atoms in each ligand. The restraints applied to each ligand were the same as described above for LiNCS·H*L*.

H atoms were positioned geometrically with C—H 0.93–0.98 and N—H 0.86 Å, and not refined. The solid-state structures of LiNCS·H*L* and CuL_2 are shown in Figs. 1 and 2, respectively. The diffraction profiles after the final bond-restrained Rietveld refinement are presented in Fig. 3.

3. Discussion

3.1. Molecular structure of CuL_2

A molecule of CuL_2 is shown in Fig. 2. Selected bond distances and angles are given in Table 2. The Cu^{II} ion is tetrahedrally coordinated by four N atoms of two bidentate ligands *L*. However, taking into consideration the relatively short distances of Cu—O24*A* [2.74 (4) Å] and Cu—O24*B* [2.64 (4) Å], one can see that O24*A* and O24*B* complete a distorted octahedral coordination sphere (Fig. 2). The Cu—N bond lengths have normal values and are in the range 1.98 (5)—2.05 (5) Å. The N—Cu—N tetrahedral angles are in the range 87 (2)–143 (2)°, while in the ZnL_2 complex the N—Zn—N angles are in the range 95.2 (4)–128.5 (6)° (Minacheva *et al.*, 2006). Considerable distortion of the CuN_4 tetrahedron is caused mainly by the formation of six-membered metallocycles with chelate angles N9*X*—Cu—N17*X* (*X* = *A* or *B*) of 94 (2) and 87 (2)° for the ligands *A* and *B*, respectively. The mean planes of two chelate rings, Cu/N9*A*/C10*A*/C15*A*/C16*A*/N17*A* and Cu/N9*B*/C10*B*/C15*B*/C16*B*/N17*B*, make a dihedral angle of 72.9 (1)°.

The conformation of the macrocyclic ring in a crown ether can be described as a sequence of conformations of ethylene glycol units: O—CH_2—CH_2—O. Each can be written as a three-letter word with the letters *T*, *C*, *G* or *S* corresponding to

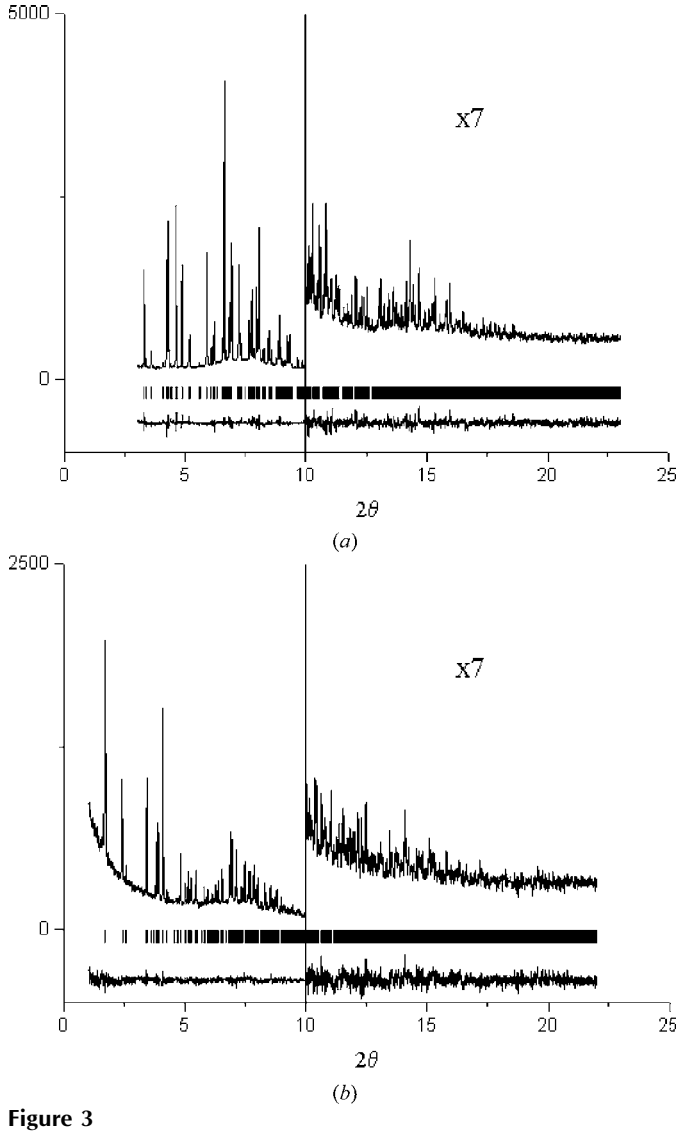

Figure 3
Rietveld plots for LiNCS·H*L* (top) and CuL_2 (bottom).

Table 3
Selected bond distances (Å) and angles (°) for LiNCS·H*L*.

Li42—O26	2.24 (3)	Li42—O33	2.50 (3)
Li42—O27	2.03 (3)	Li42—O36	2.44 (3)
Li42—O30	2.27 (3)	Li42—N41	1.98 (3)
N17—C18	1.471 (18)	N17—C16	1.338 (18)
C20—O26—Li42	108.2 (12)	C38—O26—Li42	123.9 (10)
C21—O27—Li42	115.1 (13)	C28—O27—Li42	118.5 (11)
C29—O30—Li42	102.5 (9)	C31—O30—Li42	119.1 (10)
C32—O33—Li42	116.2 (11)	C34—O33—Li42	122.6 (12)
C35—O36—Li42	120.1 (10)	C37—O36—Li42	110.3 (9)
C40—N41—Li42	165.3 (14)		

the *trans*, *cis*, *gauche* or *skew* torsional conformations, respectively. In these notations, the conformations of macrocycles in CuL_2 and ZnL_2 are described (the first word corresponds to the conformation of the O—C_{Ph}—C_{Ph}—O unit)

$$\begin{aligned} \mathrm{Cu}L_2(A): &\quad TCT\ TGT\ SST\ SGT\ GGT, \\ \mathrm{Cu}L_2(B): &\quad TCT\ TGS\ SST\ SGT\ TGT, \\ \mathrm{Zn}L_2: &\quad TCT\ TGS\ STS\ SSG\ TGT. \end{aligned}$$

In contrast to ZnL_2, the CuL_2 complex does not exhibit C_2 symmetry. As a result, the macrocycles in *A* and *B* have different conformations; however, the latter are normal for benzo-15-crown-5 (b15c5) derivatives as follows from the inspection of 123 crystal structures containing the b15c5 macrocycle in a free state (*CSD* Version 5.27; Allen, 2002).

The most striking feature of the CuL_2 crystal structure is its more dense packing compared with ZnL_2. The differences in the unit-cell volumes, 5287.7 (3) and 5760.9 (5) Å^3, lead to significantly different values of D_x (1.435 and 1.334 Mg m^{-3}) for CuL_2 and ZnL_2, respectively. *PLATON* (Spek, 2003) analysis of the two crystal structures shows the presence of voids with the volume of 150 Å^3 in ZnL_2 centered at (0.5,0,0) and symmetry-related positions, and no voids in CuL_2. However, this variation in D_x values for identical complexes is not exceptional. An illustrative example is bis((*N*-(4-methylphenyl)sulfonyl-1*H*-amido-4-isopropyl-2-phenyl)-2-oxazoline)-*M*(II), which has D_x = 1.35 Mg m^{-3} for *M* = Zn (Castro *et al.*, 2002) and D_x = 1.28 Mg m^{-3} for *M* = Co (Castro *et al.*, 2001).

3.2. LiNCS·HL structure

The molecular structure of LiNCS·H*L* is shown in Fig. 1. Selected bond distances and angles are given in Table 3. Lithium is coordinated by all five ether O atoms and the thiocyanate N atom in a distorted pentagonal pyramidal geometry. The Li42 ion is 0.38 Å above the mean plane formed by O26/O27/O30/O33/O36 with an r.m.s. deviation of 0.06 Å. The planar configuration of these O atoms is typical for b15c5 complexes with lithium and sodium salts (Kireeva *et al.*, 1991). The Li—O distances are in the range 2.03 (3)–2.50 (3) Å [average bond distance 2.30 (18) Å], which is normal for the distances between the lithium and ether O atoms (Boulatov *et al.*, 1999, and references therein). A search of the Cambridge Structural Database (Version 5.27; Allen, 2002) revealed only two crystal structures of Li complexes with b15c5 and its derivatives, namely bis(aqua(benzo-15-crown-5)-lithium)(benzo-15-crown-5))hexaiodo-tetracopper (Nurtaeva & Holt, 1999; CSD refcode BEQREU) and the toluene and tetrahydrofuran solvates of bis-(μ_4-bromo)-(12)-mercurocarborand-4)bis(aqua-(benzo-15-crown-5)lithium)-benzo-15-crown-5) (Yang *et al.*, 1994; CSD refcode LICHUA). Both compounds contain two types of 15c5 macrocycles, one of which binds to the lithium ion and another one which is free. The average Li—O distances in the b15c5 macrocycles with the bonded lithium are 2.31 and 2.25 Å in *BEQREU* and *LICHUA*, respectively. In LiNCS·H*L* the O—Li42—O angles between the neighbouring O atoms are in the range 63.5 (8)–76.3 (9)°, while the ideal angle is 72°.

The conformations of macrocycles in LiNCS·H*L* and H*L* (Minacheva, Ivanova, Dorokhov *et al.*, 2004) can be described as

$$\begin{aligned} \mathrm{LiNCS}\cdot\mathrm{H}L: &\quad TCT\ TGT\ TGT\ TGT\ TGT, \\ \mathrm{H}L: &\quad GCT\ TGT\ TGT\ TGS\ STT. \end{aligned}$$

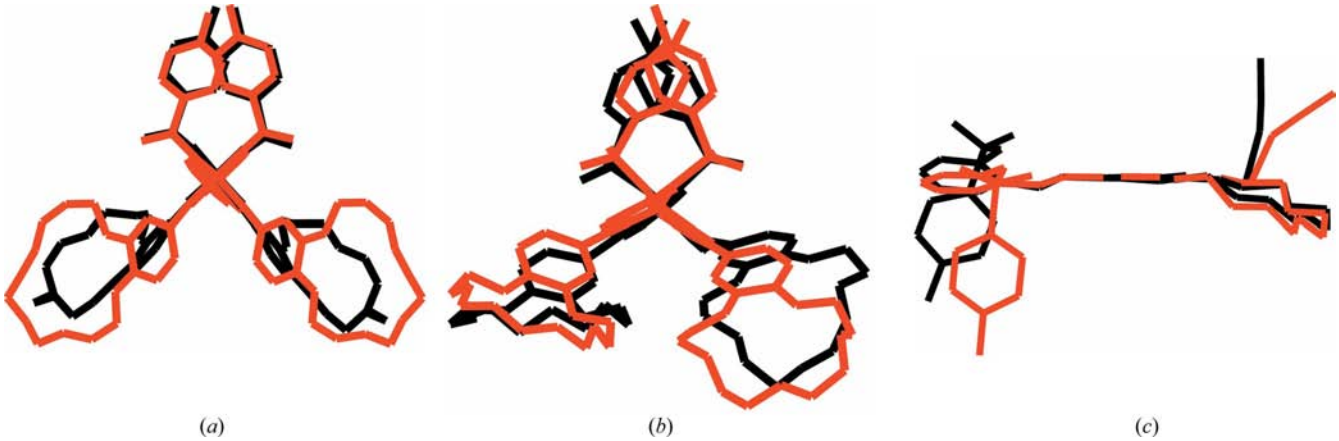

Figure 4
The comparative plots of (*a*) ZnL_2, (*b*) CuL_2 and (*c*) LiNCS·H*L* geometries after B3LYP optimization (red) and as taken from the crystal structure (black). This figure is in colour in the electronic version of this paper.

Table 4
A comparison of selected geometrical parameters (Å, °) of X-ray (first row of each line) and DFT optimized (second row of each line) complexes of ML_2 (M = Zn, Cu).

	ZnL_2	CuL_2, ligand *A*	CuL_2, ligand *B*
M—N9	2.00 (1)	1.98 (5)	1.98 (5)
	2.05	2.03	2.03
M—N17	2.05 (1)	2.05 (5)	2.03 (5)
	2.10	2.07	2.07
M—O24	2.74 (1)	2.74 (4)	2.64 (4)
	2.77	2.86	2.86
C16═N17—C18—C19	164.0 (3)	136 (7)	130 (6)
	127	134	133

Table 5
Potentiometric selectivity constants for H*L*, ZnL_2 and CuL_2.

	$\lg k^{pot}_{Pb^{2+}/ion}$		
Interfering ions	H*L*	ZnL_2	CuL_2
NH_4^+	−2.9	−3.8	+1.9
Na^+	−2.8	−3.8	−0.8
K^+	−1.5	−2.5	+2.1
Rb^+	−1.6	−3.2	−0.8
Cs^+	−2.8	−3.5	−0.8
Mg^{2+}	−2.0	−3.3	−0.2
Ca^{2+}	−2.4	−2.9	−0.4
Sr^{2+}	−1.8	−3.3	−0.2
Ba^{2+}	−2.3	−2.6	−0.1
Cu^{2+}	−1.6	−2.0	+3.3
Zn^{2+}	−2.3	−2.2	−0.2
Ag^+	−0.3	+0.8	−0.7

The symmetry of the *b*15*c*5 macrocycle in LiNCS·H*L* is higher than that in the free HL ligand, as follows from the conformations of ethylene glycol units, all of which except one ($OC_{Ph}C_{Ph}O$) transform to *TGT*. The same conformation of b15c5 was observed in its complexes with Li and Na (Kireeva *et al.*, 1991).

3.3. Comparison of CuL_2 and ZnL_2 complexes

A comparison of CuL_2 and ZnL_2 shows different conformations of the crowns in each molecule in the crystalline state. Even the two crowns in two ligands of CuL_2 have different conformations. The data suggest that the differences in ion selectivity for CuL_2 and ZnL_2 may be related to the hole size, *i.e.* when the crown ether's interior cavity ('hole') is about the same size as a given cation, binding will be optimal. However, it should be noted that the idea of hole size is not a principle that can be applied universally (Gokel *et al.*, 2004). Moreover, the X-ray structure is essentially static; the crystal packing effects may significantly influence the molecular geometry, while complexation, or ion binding, typically occurs in a solvent.

To understand why the conformations of CuL_2 and ZnL_2 in the solid state are different and to estimate their probable geometries in a solution, we carried out a computational investigation of these complexes by DFT using the X-ray structures as input geometries. The minimum-energy geometries calculated for ZnL_2 and CuL_2 are shown in Fig. 4 along with their X-ray geometries. Both calculated structures show some elongation of the *M*—N coordinating bond lengths (Table 4). In ZnL_2 the DFT optimization basically preserves the C_2 symmetry of the molecule, but causes a significant rotation of the b15c5 moiety around the N17—C18 bond. The torsion angle C═N—C—C changes from 164.0 (7)° in the X-ray structure to 127° in the complex optimized *in vacuo*. In the CuL_2 complex there are no changes in this torsion angle in either ligands within experimental error (Table 4) and the values of this angle in both ligands of the DFT optimized complex (133 and 134°) are close to that in the ZnL_2 complex (127°).

In the crystal structure of ZnL_2 the high value of the torsion angle C═N—C—C indicates that two benzene rings (C10–C15 and C18–C23) are nearly parallel in each ligand. This conformation is energetically unfavourable *in vacuo*, as follows from the geometries of the DFT optimized complexes ZnL_2 and CuL_2, but in the crystal (where weak intermolecular forces may influence molecular geometry) we observe just this unfavourable conformation, which is, however, favourable for the $\pi\cdots\pi$ stacking formation. Indeed, in the crystal packing of ZnL_2 $\pi\cdots\pi$ interactions exist which link the molecules into ribbons with the short distance of 3.650 (5) Å between the centroids of the benzene rings C10–C15 and C18–C23 from the neighbouring molecules (Fig. 5). Further packing of these ribbons with the protruding macrocycles in the crystal leads to a porous packing with considerable voids; this explains the existence of voids with a volume of 150 $Å^3$ in ZnL_2 crystal packing.

The essential difference in the values of the torsion angle C═N—C—C in the crystal and *in vacuo* optimized ZnL_2 indicates a weak interaction of the b15c5 macrocycle with the rest part of the molecule in the ML_2 complex; this allows easy rotation of b15c5 around the N17—C18 bond. Another

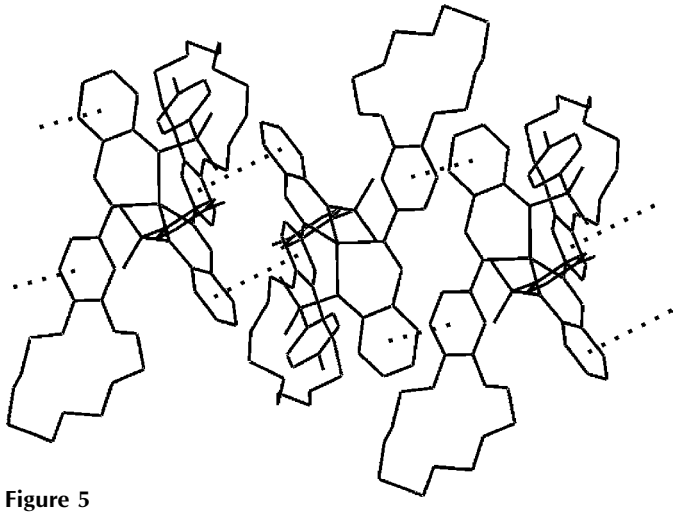

Figure 5
The $\pi\cdots\pi$ interactions (dotted lines) in the crystal structure of ZnL_2. The distances between the centroids of benzene rings from the neighbouring molecules are 3.650 (5) Å.

important conclusion is that the macrocycle conformation is almost independent of the nature of the central *M* ion. The central *M* ion defines the geometry of that part of the ligand which coordinates it, namely, the 2-(amino-*N*-tosyl)phenylaldimine (*L*′). The geometries of ML'_2 fragments are qualitatively the same in X-ray and *in vacuo* optimized systems of ZnL_2 and CuL_2 (Fig. 4).

The Cu/N9/C10–C16/N17 fragment is distorted from planarity in both ligands of the DFT-optimized CuL_2 complex – the maximal deviations from the mean plane in ligand *A* are −0.13 and 0.18 Å for the Cu and N9*A* atoms, respectively, and in ligand *B* the same deviations are −0.16 and 0.19 Å for the Cu and N9*B* atoms, respectively. These two mean planes form a dihedral angle of 65°. The same atomic fragment in DFT-optimized ZnL_2, Zn/N9/C10–C16/N17, is almost planar – the maximal deviations from the mean planes in the two ligands do not exceed 0.04 Å. However, the most important distinction from the CuL_2 complex is the almost perpendicular orientation of the two mean planes, with a dihedral angle of 89°. The value of this dihedral angle defines the dimensions of the 'access' area, where an ion has the opportunity to bind to the macrocycle without steric obstacles (caused by the C10–C15 benzene ring and O24 atom from another ligand) – the closer to 90° the larger the 'access' area. If this assumption is valid, the potentiometric selectivity constants $k^{\rm pot}_{\rm Pb^{2+}/ion}$ for ZnL_2 are to correspond with those for H*L*, which has a maximal possible 'access' area, and experimental measurements of transport properties in PVC membranes show this tendency (Table 5).

The variety of b15c5 conformations observed in the ligands of both complexes in the solid state and optimized *in vacuo* clearly shows that in ML_2 solution, the macrocycle should be considered to be flexible and capable of orienting three of its five donor groups in space. However, as soon as the macrocycle binds an ion, its conformation becomes more rigid and can be predicted by DFT calculations with a good precision, as has been shown by Platas-Iglesias and co-workers (Platas-Iglesias, Vaiana *et al.*, 2005; Platas-Iglesias, Esteban-Gómez *et al.*, 2005). To be sure that this statement is valid for our compounds, we carried out a DFT geometry optimization of the LiNCS·H*L* complex, where the macrocycle binds a lithium ion. A comparison of the X-ray and *in vacuo* optimized geometries of LiNCS·H*L* (Fig. 4*c*) revealed that the macrocycle conformation and the positions of Li and coordinating N atoms suffer only very small variations, in spite of the considerable displacements of the tosyl group and the S atom from the thiocyanate moiety.

3.4. Conformational flexibility of the ligand H*L*

The conclusions that the macrocycle in the ML_2 complex should be considered flexible and that its conformation is almost independent of the nature of the central *M* atom have stimulated us to optimize the geometries of several H*L* ligands *in vacuo* to compare their conformations and relative energies. The five input geometries of H*L* ligands were taken from the crystal structures of H*L*, LiNCS·H*L*, ZnL_2 (one independent ligand) and CuL_2 (two independent ligands). The *in vacuo* optimized geometries were compared to the input X-ray values in Fig. 6. The differences in the energies for the five optimized geometries do not exceed 16 kJ mol^{-1}, allowing various conformations of the macrocycle and giving no preference to any in particular.

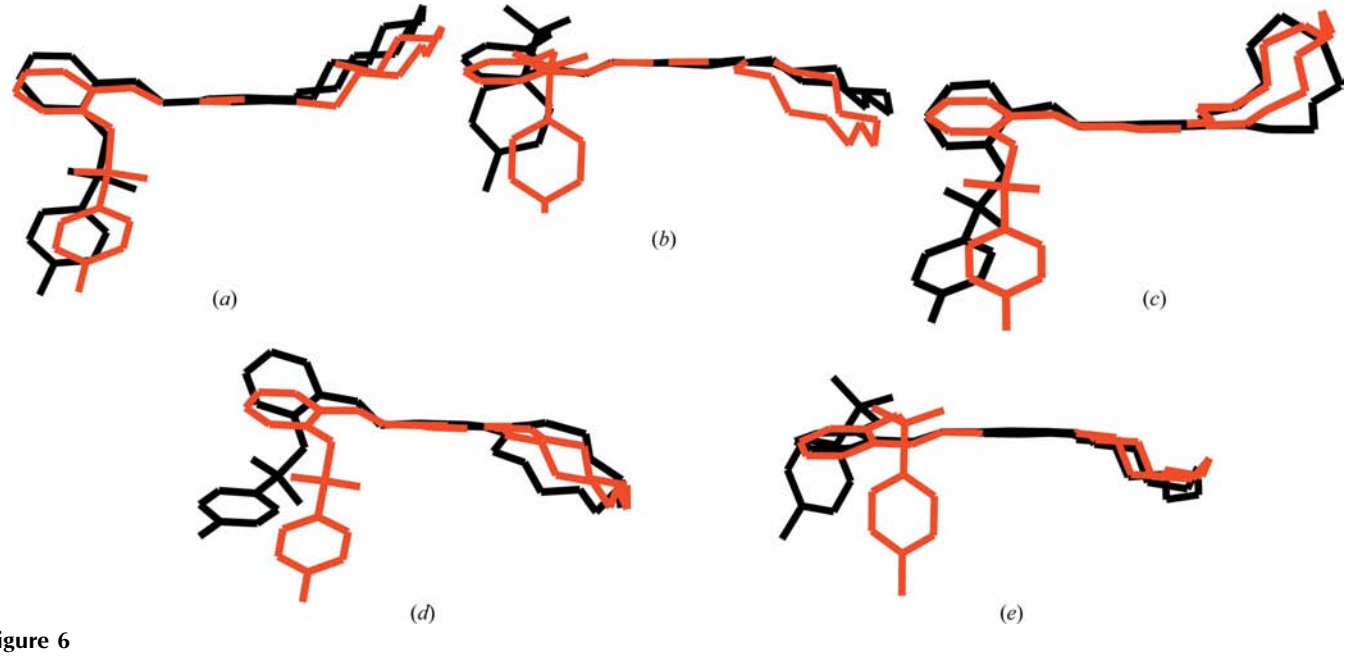

Figure 6
The comparative plots of H*L* geometries after B3LYP optimization (red) and as taken from the crystal structure (black) of (*a*) H*L*, (*b*) LiNCS·H*L*, (*c*) CuL_2 ligand *A*, (*d*) CuL_2 ligand *B* and (*e*) ZnL_2. This figure is in colour in the electronic version of this paper.

4. Conclusion

A comparison of X-ray and DFT optimized geometries of two complexes, CuL_2 and ZnL_2, allowed us to identify the relatively rigid ML'_2 fragments [L' = 2-(amino-*N*-tosyl)phenylaldimine] in the molecules. The geometry of this ML'_2 fragment depends on the electronic structure of the metal ion *M*, which determines the geometry of the MN_4 coordination tetrahedron and the spatial orientation of b15c5 macrocycles in ML_2 complexes. The differences in spatial orientations of b15c5 macrocycles in CuL_2 and ZnL_2 complexes qualitatively explain the difference in their potentiometric selectivities. The results allow further computational study of various ML_2 complexes with two bonded ions – the rigidity of the ML'_2 fragment and the conformation of the macrocycle with the bonded ion provide a good basis for such time-consuming *ab initio* calculations.

The authors thank the staff of the SNBL for their friendly support during the synchrotron experiments and Professor A. V. Yatsenko for his kind assistance with DFT calculations.

References

Allen, F. H. (2002). *Acta Cryst.* B**58**, 380–388.

Amini, A. (2001). *Electrophoresis*, **22**, 3107–3130.

Baerlocher, Ch. & McCusker, L. B. (2004). Editors. *Z. Kristallogr.* **219**, 782–901.

Bakker, E., Bühlmann, P. & Pretsch, E. (1997). *Chem. Rev.* **97**, 3083–3132.

Becke, A. D. (1988). *Phys. Rev. A*, **38**, 3098–3100.

Bell, T. W. & Hext, N. M. (2004). *Chem. Soc. Rev.* **33**, 589–598.

Boulatov, R., Du, B., Meyers, E. A. & Shore, S. G. (1999). *Inorg. Chem.* **38**, 4554–4558.

Bren, V. A. (2001). *Russ. Chem. Rev.* **50**, 1017–1034.

Bühlmann, P., Pretsch, E. & Bakker, E. (1998). *Chem. Rev.* **98**, 1593–1687.

Castro, J., Cabaleiro, S., Perez-Lourido, P., Romero, J., Garcia-Vazquez, J. A. & Sousa, A. (2001). *Polyhedron*, **20**, 2329–2337.

Castro, J., Cabaleiro, S., Perez-Lourido, P., Romero, J., Garcia-Vazquez, J. A. & Sousa, A. (2002). *Z. Anorg. Allg. Chem.* **628**, 1210–1217.

Chernyshev, V. V. & Schenk, H. (1998). *Z. Kristallogr.* **213**, 1–3.

Cook, H. A., Klampfl, C. W. & Buchberger, W. (2005). *J. Chromatogr. A*, **1085**, 164–169.

Dale, J., Eggestad, J., Fredriksen, S. B. & Groth, P. (1987). *Chem. Commun.* pp. 1391–1392.

David, W. I. F., Shankland, K., McCusker, L. B. & Baerlocher, Ch. (2002). Editors. *Structure Determination from Powder Diffraction Data*. New York: Oxford University Press.

Dollase, W. A. (1986). *J. Appl. Cryst.* **19**, 267–272.

Fedorova, O. A., Gromov, S. P. & Alfimov, M. V. (2001). *Russ. Chem. Bull.* **50**, 1970–1983.

Gokel, G. W., Leevy, W. M. & Weber, M. E. (2004). *Chem. Rev.* **104**, 2723–2750.

Gonzalez-Lorenzo, M., Platas-Iglesias, C., Avecilla, F., Geraldes, C. F. G. C., Imbert, D., Bünzli, J.-C. G., De Blas, A. & Rodriguez-Blas, T. (2003). *Inorg. Chem.* **42**, 6946–6954.

Ha, P. T., Hoogmartens, J. & Van Schepdael, A. (2006). *J. Pharm. Biomed. Anal.* **41**, 1–11.

Inoue, Y. & Gokel, G. W. (1990). Editors. *Cation Binding by Macrocycles.* NY: Marcell Dekker.

International Union of Crystallography Newsletter (2004). Vol. 31, pp. 5–15. NY: IUCr.

IUPAC Recommendation for Nomenclature of Ion Selective Electrodes (1976). *Pure Appl. Chem.* **48**, 127.

Ivanova, I. S., Dorokhov, A. V., Pyatova, E. N., Bicherov, A. V., Burlov, A. S., Garnovskii, A. D. & Tsivadze, A. Yu. (2005). *Russ. J. Coord. Chem.* **31**, 483–488.

Ivanova, I. S., Dorokhov, A. V., Pyatova, E. N., Burlov, A. S., Garnovskii, A. D. & Tsivadze, A. Yu. (2007*a*). *Russ. J. Coord. Chem.* In the press.

Ivanova, I. S., Dorokhov, A.V., Pyatova, E. N., Burlov, A. S., Garnovskii, A. D. & Tsivadze, A. Yu. (2007*b*). *Russ. J. Coord. Chem.* In the press.

Izatt, R. M. & Christensen, J. J. (1978). Editors. *Synthetic Multidentate Macrocyclic Compounds.* NY: Academic Press.

Kireeva, I. K., Generalova, N. B., Trofimov, V. A. & Tsivadze, A. Yu. (1991). *Russ. J. Inorg. Chem.* **36**, 830–838.

Laikov, D. N. (1997). *Chem. Phys. Lett.* **281**, 151–156.

Lee, C. T., Yang, W. T. & Parr, R. G. (1988). *Phys. Rev. B*, **37**, 785–789.

Liu, Y., Zhang, H.-Y., Chen, L.-X., He, X.-W., Wada, T. & Inoue, Y. (2000). *J. Org. Chem.* **65**, 2870–2874.

Mazik, M., Kuschel, M. & Sicking, W. (2006). *Org. Lett.* **8**, 855–858.

Minacheva, L. Kh., Ivanova, I. S., Dorokhov, A. V., Bicherov, A. V., Burlov, A. S., Garnovskii, A. D., Sergienko, V. S. & Tsivadze, A. Yu. (2004). *Dokl. Chem.* **398**, 179–184.

Minacheva, L. Kh., Ivanova, I. S., Dorokhov, A. V., Burlov, A. S., Garnovskii, A. D., Sergienko, V. S. & Tsivadze, A. Yu. (2006). *Russ. J. Coord. Chem.* **32**, 166–172.

Minacheva, L. Kh., Ivanova, I. S., Pyatova E. N., Dorokhov, A. V., Bicherov, A. V., Burlov, A. S., Garnovskii, A. D., Sergienko, V. S. & Tsivadze, A. Yu. (2004). *Dokl. Chem.* **395**, 68–73.

Nurtaeva, A. & Holt, E. M. (1999). *Acta Cryst.* C**55**, 1453–1457.

Pawley, G. S. (1981). *J. Appl. Cryst.* **14**, 357–361.

Platas-Iglesias, C., Esteban-Gómez, D., Enríquez-Pérez, T., Avecilla, F., de Blas, A. & Rodriguez-Blas, T. (2005). *Inorg. Chem.* **44**, 2224–2233.

Platas-Iglesias, C., Vaiana, L., Esteban-Gómez, D., Avecilla, F., Real, J. A., de Blas, A. & Rodriguez-Blas, T. (2005). *Inorg. Chem.* **44**, 9704–9713.

Popa, N. C. (1998). *J. Appl. Cryst.* **31**, 176–180.

Shimojo, K., Nakashima, K., Kamiya, N. & Goto, M. (2006). *Biomacromolecules*, **7**, 2–5.

Sousa, C., Gameiro, P., Freire, P. & de Castro, B. (2004). *Polyhedron*, **23**, 1401–1408.

Spek, A. L. (2003). *J. Appl. Cryst.* **36**, 7–13.

Toraya, H. (1986). *J. Appl. Cryst.* **19**, 440–447.

Tsivadze, A. Yu. (2004). *Russ. Chem. Rev.* **73**, 5–23.

Van Veggel, F. C. J. M., Verboom, W. & Reinhoudt, D. N. (1994). *Chem. Rev.* **94**, 279–299.

Visser, J. W. (1969). *J. Appl. Cryst.* **2**, 89–95.

Werner, P.-E., Eriksson, L. & Westdahl, M. (1985). *J. Appl. Cryst.* **18**, 367–370.

Yang, X., Knobler, C. B., Zheng, Z. & Hawthorne, M. F. (1994). *J. Am. Chem. Soc.* **116**, 7142–7159.

Young, R. A. & Wiles, D. B. (1982). *J. Appl. Cryst.* **15**, 430–438.

Zhukov, S. G., Chernyshev, V. V., Babaev, E. V., Sonneveld, E. J. & Schenk, H. (2001). *Z. Kristallogr.* **216**, 5–9.

Zlokazov, V. B. (1992). *J. Appl. Cryst.* **25**, 69–72.

Zlokazov, V. B. (1995). *Comput. Phys. Commun.* **85**, 414–422.

Zlokazov, V. B. & Chernyshev, V. V. (1992). *J. Appl. Cryst.* **25**, 447–451.